ACS OMEGA

http://pubs.acs.org/journal/acsodf

Article

# Silica-Coated Magnetic Nanoparticles for Vancomycin Conjugation

Moustafa M. Abdelaziz, Amr Hefnawy, Asem Anter, Menna M. Abdellatif, Mahmoud A. F. Khalil, and Islam A. Khalil*

Cite This: *ACS Omega* 2022, 7, 30161−30170

Read Online

ACCESS | Metrics & More | Article Recommendations



**ABSTRACT:** Drug resistance is a global health challenge with thousands of deaths annually caused by bacterial multidrug resistance (MDR). Efforts to develop new antibacterial molecules do not meet the mounting needs imposed by the evolution of MDR. An alternative approach to overcome this challenge is developing targeted formulations that can enhance the therapeutic efficiency and limit side effects. In this aspect, vancomycin is a potent antibacterial agent that has inherent bacterial targeting properties by binding to the D-Ala-D-Ala moiety of the bacterial peptidoglycan. However, the use of vancomycin is associated with serious side effects that limit its clinical use. Herein, we report the development of vancomycin-conjugated magnetic nanoparticles using a simple conjugation method for targeted antibacterial activity. The nanoparticles were synthesized using a multistep process that starts by coating the nanoparticles with a silica layer, followed by binding an amide linker and then binding the vancomycin glycopeptide. The developed vancomycin-conjugated magnetic nanoparticles were observed to exhibit a spherical morphology and a particle size of 16.3 ± 2.6 nm, with a silica coating thickness of 5 nm and a total coating thickness of 8 nm. The vancomycin conjugation efficiency on the nanoparticles was measured spectrophotometrically to be 25.1%. Additionally, the developed formulation retained the magnetic activity of the nanoparticles, where it showed a saturation magnetization value of 51 emu/g, compared to 60 emu/g for bare magnetic nanoparticles. The in vitro cell biocompatibility demonstrated improved safety where vancomycin-conjugated nanoparticles showed $IC_{50}$ of 183.43 $\mu$g/mL, compared to a much lower value of 54.11 $\mu$g/mL for free vancomycin. While the antibacterial studies showed a comparable activity of the developed formulation, the minimum inhibitory concentration was 25 $\mu$g/mL, compared to 20 $\mu$g/mL for free vancomycin. Accordingly, the reported formulation can be used as a platform for the targeted and efficient delivery of other drugs.

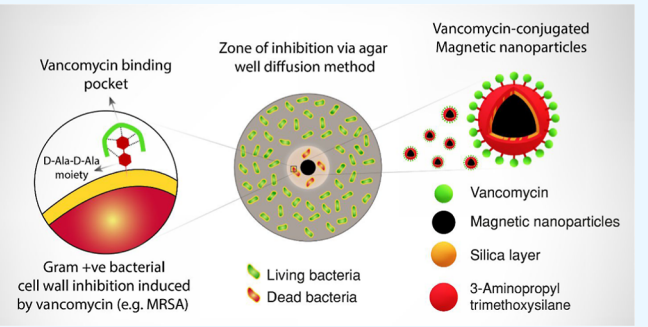


## 1. INTRODUCTION

Bacterial multidrug resistance (MDR) is one of the serious challenges to the public health. Several bacterial species showed resistance to broad antibiotics such as methicillin-resistant *Staphylococcus aureus* (MRSA), which limits the available options to fight such virulent bacteria.[1] UK authorities estimated the mortality rate due to MDR to reach 700,000 per year, and the number is expected to increase to 10 million by 2050 if no substantial solution exists.[2] Therefore, there is a necessity for more efficient antibacterial strategies that can eradicate MDR. Conventional approaches such as developing new drugs cannot accommodate the steady increase in bacterial resistance due to its long development time and massive cost. New strategies have been proposed to circumvent MDR such as nanomaterial-based drug delivery vehicles which confer the advantage of localizing the drug administration. Therefore, drug concentration is accumulated in the infection site, while the off-target toxicity can be averted.[3] In addition, some nanoparticles (NPs) (e.g., metal NPs) could overcome the mechanisms of MDR by disrupting the bacterial membrane and preventing biofilm formation, thereby making bacteria more susceptible to the loaded antibiotics.[4−7]

Glycopeptides (GPs) are a preferred class of antibiotics as they induce less bacterial resistance compared to traditional antibiotics due to exhibiting multiple action modes.[8] Most of the GPs are usually derived from a natural source, which confers the advantage of biocompatibility and biodegradability.[9,10] The GPs' bactericidal mode of action relies on their unique structure, which includes net positive charge residues. Therefore, GPs could electrostatically interact with the negatively charged bacterial cell membranes leading to the disruption of bacterial membranes.[11] For instance, vancomycin

Received: May 24, 2022
Accepted: August 3, 2022
Published: August 16, 2022

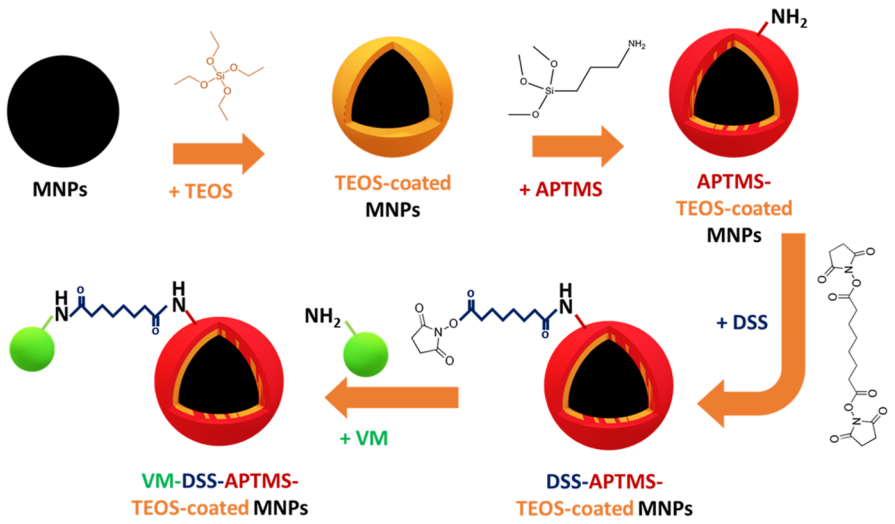


**Figure 1.** Schematic illustration of the developed nano-in-micro inhalable formulation, MNPs: magnetic nanoparticles, TEOS: tetraethyl orthosilicate, APTMS: (3-aminopropyl)trimethoxysilane, DSS: disuccinimidyl suberate, and VM: vancomycin.

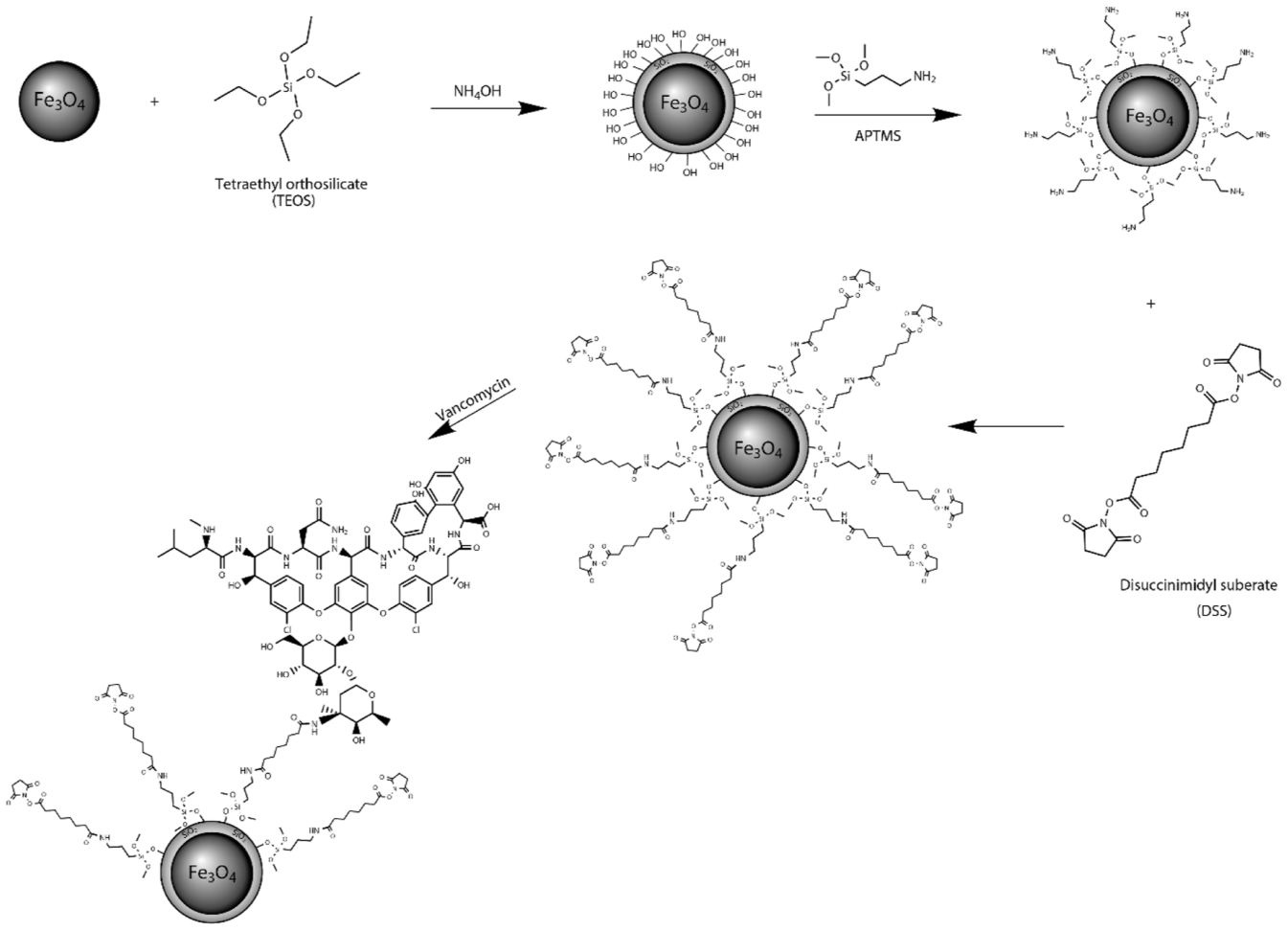


**Figure 2.** Schematic diagram for the synthetic steps of VM-conjugated MNPs. MNPs ($Fe_3O_4$): magnetic nanoparticles, TEOS: tetraethyl orthosilicate, APTMS: (3-aminopropyl)triethoxysilane, DSS: disuccinimidyl suberate, and VM: vancomycin.

(VM) is usually used in surgery practices to reduce the incidence of perioperative bacterial infections such as MRSA infections.[12−14] VM can inhibit the bacterial cell wall synthesis by interfering with the bacterial transpeptidase.[15,16] This inhibition is initiated through VM binding to the D-Ala-D-Ala terminal in peptidoglycans.[17] Recently, D-Ala-D-Ala binding has been exploited as a targeting moiety for VM because it is only present in the bacterial cell wall. However, the free administration of VM was reported to be associated with some adverse effects including nephrotoxicity,[18] ototox-



https://doi.org/10.1021/acsomega.2c03226
ACS Omega 2022, 7, 30161−30170

icity,[19] and red man syndrome.[20] A potential solution to this problem is the incorporation of VM into a targeted drug delivery vehicle, which can localize the VM and reduce the associated side effects.

Iron oxide magnetic nanoparticles (MNPs) are an example of the smart vehicles that has been exploited for drug delivery applications. The unique magnetic properties of these MNPs confer wide use in various biomedical applications either diagnostically as a contrasting agent, therapeutically as a hyperthermia agent, or both combined as in the theranostics approach.[21−23] MNPs can target the loaded drug to the infection site when guided by an external magnet. MNPs may also contribute to the overall antibacterial character due to their capability to generate cytotoxic hyperthermia when induced by an alternating magnetic field. Moreover, MNPs can be functionalized with a proper antibiotic to confer both a synergistic efficiency and a selective action.[24] Functionalization was also reported to enhance the biocompatibility and the colloidal stability of MNPs.[25]

Functionalized MNPs are designed to have better selectivity, bactericidal activity, and biocompatibility while maintaining the magnetic properties. Such functionalization can be performed either by physically entrapping VM on properly coated MNPs or chemically conjugating VM on the surface of MNPs. For instance, Zhang et al. utilized a polymeric coating of polyvinyl alcohol (PVA) to entrap VM on MNPs.[26] At first, MNPs were stabilized by a silica layer which also allows for more hydroxyl functional groups. Then, PVA was melted and added to the silica-coated MNPs. This core−shell system was further conjugated with a chain of cell penetrating peptides to facilitate its cellular internalization. The resulting system showed targeted antibacterial activity against Gram-positive and Gram-negative bacterial strains with a lower VM dose than used in its free form. Rashid et al.[27] have reported the chemical conjugation of VM on MNPs via ligand exchange and carbodiimide reactions. Briefly, they first coated MNPs with oleic acid as stabilizer, and then oleic acid was replaced with the amine-ending dopamine to improve the water dispersion of MNPs. Then, VM was conjugated to the dopamine-modified MNPs via a carbodiimide reaction. The resulting conjugate demonstrated bactericidal activity to Gram-positive and Gram-negative strains with high affinity to the bacterial cell walls.

Herein, we report the development of VM-conjugated MNPs (VMNPs). Chemical conjugation allows the dual use of MNPs and VM for targeted antibacterial activity. On the one hand, an external magnetic field can be applied to localize the antibacterial formulation at the targeted organ and minimize the amount leaking into the systemic circulation. Meanwhile, having VM conjugated to the surface of the MNPs can also allow targeting of the bacteria on the cellular level due to its binding affinity to the D-Ala-D-Ala residues in the bacterial cell wall.[28] Thus, VM delivery is localized which can lower the required VM dose, limit biodistribution, and minimize the VM's off-site toxicity. The biocompatibility of the developed VMNPs was assessed on normal lung cells, while the antibacterial activity was examined against *Staphylococcus aureus* (*S. aureus*) and MRSA (Figure 1).

## 2. MATERIALS AND METHODS

**2.1. Materials.** Iron(III) chloride anhydrous, 98% ($FeCl_3$) was purchased from Fischer Scientific (Waltham, MA, USA). (3-Aminopropyl)trimethoxysilane 97% (APTMS), dimethyl sulfoxide (DMSO), iron(II) chloride anhydrous ($FeCl_2$), and tetraethyl orthosilicate (TEOS) were purchased from Sigma-Aldrich (Gillingham, UK). Disuccinimidyl suberate, 97% (DSS), and VM hydrochloride (Molecular Biology Grade) were obtained from Alfa Aesar (Haverhill, MA, USA). Ammonia 30−33 wt % solution ($NH_3$) and ethanol absolute (EtOH) were obtained from Chem-Lab NV (Zedelgem, Belgium).

**2.2. Synthesis of VM-Conjugated MNPs.** The synthesis procedure of VMNPs is a multi-step process (Figure 2) that could be summarized as follows:

*2.2.1. Preparation of the MNPs.* Following a co-precipitation method, 5 mol $FeCl_2$ and 10 mol $FeCl_3$ were dissolved in deoxygenated water at 70 °C under vigorous stirring. Then, ammonia (30−33 wt %) solution was added (30 mL) at a rate of 6 mL/min to the mixture under bath sonication and nitrogen flushing. Upon the addition of the ammonia, a black precipitate of MNPs began to form which was gathered using a strong magnet. Afterward, the supernatant was removed and MNPs were washed several times with distilled water and ethanol to ensure the removal of any unreacted materials.[29]

*2.2.2. Coating of the MNPs by a Silica Layer.* The coating of MNPs with silica was conducted following a modified reported procedure.[30] MNPs (1 g) were suspended in 100 mL of absolute ethanol under bath sonication (ELMA, Germany) for 30 min. Then, 10 mL of ammonia (30−33 wt %) solution and 80 mL of Milli-Q water were added in a drop-wise manner. TEOS (0.5 mL) was also added to the suspension under sonication for 2 h, soaked overnight, and sonicated again for 6 h. The TEOS-coated MNPs were separated using magnetic decantation and washed repeatedly with ethanol and Milli-Q water.

*2.2.3. Functionalization of the Silica-Coated MNPs.* The objective of adding APTMS is to functionalize the surface of the silica layer with $NH_2$ groups that would be used later to conjugate VM. To do so, TEOS-coated MNPs were dispersed in a mixture of 50 mL of ethanol and 1 mL of HCl to acidify the media. Then, 5 mL of APTMS was added dropwise to the dispersion under sonication for 4 h. To separate the APTMS−TEOS-coated MNPs, the dispersion was centrifuged (refrigerated high-speed centrifuge, Sigma 3-30k, Germany) at 19,000*g* for 15 min and the supernatant was removed. Thereafter, the precipitate was washed multiple times with ethanol and distilled water, each time was followed by centrifugation at 19,000*g* for 15 min.

*2.2.4. Conjugation of VM on the Silica-Coated MNPs.* The conjugation of VM on APTMS−TEOS-coated MNPs was achieved with the aid of the double crosslinker DSS.[31] At first, 50 mg of DSS was dissolved in 50 mL of DMSO while stirring. Then, 50 mg of APTMS−TEOS-coated MNPs was dispersed in the DSS solution using a homogenizer for 1 h. To separate the product, the dispersion was centrifuged at 19,000*g* for 15 min and the product was rinsed 3−4 times with ethanol and distilled water. DSS-activated-MNPs were dispersed in 50 mL of VM solution (0.5 mg/mL) under homogenization at 4 °C for 12 h. The dispersion was centrifuged (19,000*g*, 4 °C, and 15 min) and washed repeatedly with ethanol and distilled water. In the end, the freshly prepared VM−DSS−APTMS−TEOS-coated MNPs (VMNPs) were frozen and lyophilized to get the final product in a powder form.

**2.3. Characterization.** A Fourier transform infrared (FTIR) spectrometer (Shimadzu IR-Affinity-1, Japan) was used to confirm each separate step followed during the



https://doi.org/10.1021/acsomega.2c03226
ACS Omega 2022, 7, 30161−30170

synthesis of VMNPs. High-resolution transmission electron microscopy (HR-TEM) (JEM-2100, JEOL Ltd. Japan) was utilized to observe the size and crystalline structure of MNPs, besides the confirmation of the $SiO_2$ layers coating. A vibrating sample magnetometer (VSM) (Lake Shore model 7410, USA) was used to assess the difference in magnetization saturation value of MNPs before and after functionalization. The size and charge of the VMNPs were determined using a zetasizer (Nano-ZS, Malvern Instruments, Malvern, UK). Regarding the iron content of MNPs, inductively coupled plasma atomic emission spectroscopy [Agilent 5100 Synchronous Vertical Dual View (SVDV) ICP-OES, CA, USA] was utilized to determine such an amount. Thermogravimetric analysis (TGA) (SDT, Q600, TA Instruments, USA) was used to confirm the successful functionalization of MNPs and to measure their thermal stability. For VM, a UV−vis spectrophotometer (Shimadzu UV 1650 spectrophotometer, Japan) was used to determine the conjugation efficiency at 279.8 nm.

**2.4. Conjugation Efficiency.** The amount of conjugated VM on MNPs was determined indirectly using a UV−vis spectrophotometer (Shimadzu UV 1650 spectrophotometer, Japan). After the VMNPs were prepared, centrifuged, washed, and isolated, the supernatant was taken for the analysis of unconjugated VM at 279.8 nm. The conjugation efficiency (CE %) of VM was calculated as follows

$$\text{CE } \% = \frac{m_{\text{initial}} - m_{\text{supernatant}}}{m_{\text{initial}}} \times 100$$

where $m_{\text{initial}}$ expresses the initial mass of VM and $m_{\text{supernatant}}$ expresses the amount of VM found in the supernatant. It is worthy to mention that $m_{\text{supernatant}}$ value is determined from the calibration curve of VM at 279.8 nm.

The loading efficiency (LE %) of VM is also calculated by dividing the conjugated amount of VM, given from CE % calculation ($m_{\text{initial}} - m_{\text{supernatant}}$), over the total VMNP yield.

**2.5. Cell Biocompatibility Assay.** *2.5.1. WI-38 Cell Culture Protocol.* The cell line used in this study was WI-38 human diploid lung fibroblast which was obtained from the American Type Culture Collection (Manassas, VA, USA). The growth of WI-38 cells was carried out in DMEM (Invitrogen/Life Technologies) which was supplemented with 10% fetal bovine serum (Hyclone, USA), 10 $\mu$g/mL insulin (Sigma-Aldrich, USA), and 1% penicillin−streptomycin. The cells were transferred to a 96-well plate ($1.2-1.8 \times 10^4$ cells/well) in which a volume of 100 $\mu$L of complete growth medium and 100 $\mu$L of the VMNP suspension was added to each well for 24 h incubation prior to the MTT assay.

*2.5.2. Biocompatibility Assessment Using the MTT Assay.* The biocompatibility profile of the developed VMNPs was examined in vitro using the MTT assay. The viability of tested cells could be quantitatively measured from the optical density of formed blue formazan crystals using an appropriate spectrophotometer. Briefly, viable cells are particularly capable of cellularly reducing MTT yellow molecules into the purple formazan crystals. The testing protocol is performed as reported by the manufacturer's instructions (Sigma-Aldrich, MO, USA). In brief, WI-38 cell culture with the testing VMNPs was moved to a laminar flow hood. Immediately, each vial of MTT [M-5655] was added to each well with an equivalent amount of 10% of the well medium volume. The cell culture with MTT was then incubated for 3 h at 37 °C to allow the reaction to proceed. Afterward, the combination was transferred out of incubation and the produced formazan crystals were dissolved with the solubilization solution [M-8910] using an automated shaker. The formazan solution was analyzed using ROBONIK P2000 spectrophotometer 450 nm reader, in which the absorbance of formazan color was detected at 570 nm and the background absorbance was detected at 690 nm. Cell viability percentage could be inferred by comparing the optical density values of control cells and tested cells.

**2.6. Antibacterial Activity Evaluation.** The antimicrobial activity was carried out using agar well diffusion as previously reported.[32] Briefly, *S. aureus* and MRSA were subjected to antimicrobial susceptibility testing to detect antimicrobial activity of the formula prepared. Profiling was performed by the agar well diffusion method on a Mueller−Hinton agar according to Clinical and Laboratory Standards Institute guidelines. An inoculum for each isolate was prepared by emulsifying colonies from an overnight pure culture in sterile normal saline (0.85%) in test tubes with the turbidity adjusted to 0.5 McFarland standard (0.5 mL of 1% w/v $BaCl_2$ and 99.5 mL of 1% v/v $H_2SO_4$), equivalent to $1.0 \times 10^8$ cfu/mL. The bacterial suspension was uniformly streaked on Mueller Hinton agar plates using sterile swabs and left for 3 min prior to introduction of the diluted formula. Then, a hole with a diameter of 6 to 8 mm is punched aseptically with a sterile cork borer or a tip, and a volume (20−100 $\mu$L) of the antimicrobial agent or extract solution at desired concentration is introduced into the well. Then, agar plates are incubated at 35 °C for 24 h. The antimicrobial agent diffuses in the agar medium and inhibits the growth of the microbial strain tested, and the diameters of zone of inhibition were measured and results interpreted according to Clinical Laboratory Standards Institute.[33] The method was used to measure the inhibition zones, which were reported in millimeters. The minimum inhibition diameter represents the minimum inhibitory concentration (MIC). The test samples were examined against *S. aureus* (ATCC 25923) and MRSA (ATCC 43300). VM was used as a positive standard and all measurements were conducted in a triplicate manner. The followed procedure started with the inoculation of bacterial strains on nutrient agar plates using a sterile cotton swab under aseptic conditions. Afterward, 100 $\mu$L of VMNP samples (at concentration range 15−400 $\mu$g/mL) was added to a corresponding well (10 mm) and incubated at 37 °C for 24 h. To depict the antibacterial activity of the samples, the diameter of each inhibition zone was measured and compared to each other.

**2.7. Statistical Analysis.** Data are expressed as means ± standard error from three replicate experiments. Significant differences were examined by one-way analysis of variance followed by Tukey's posthoc tests (*$p < 0.05$, **$p < 0.01$, ***$p < 0.001$ and ****$p < 0.0001$) using the software GraphPad Prism Software version 6.

## 3. RESULTS AND DISCUSSION

The study developed VM-conjugated formulation to achieve comparable activity to free VM, while having a better biocompatibility profile. This was done by conjugating VM to MNPs utilizing the targeting capability of both components for a localized antibacterial activity. Initially, we characterized the physicochemical properties of the developed VMNPs to confirm the suitability of the formulation to the intended application. These characterization analyses included composition, morphology, magnetic, and thermal analyses. Afterward,


https://doi.org/10.1021/acsomega.2c03226
ACS Omega 2022, 7, 30161−30170

the biocompatibility and the antibacterial activity of the formulation were evaluated in comparison to free VM.

**3.1. Physicochemical Properties of NPs.** VM-conjugated MNPs were characterized to ensure the successful chemical conjugation of VM on MNPs, assess the size and morphology of NPs, evaluate the thermal behavior of NPs, and study the magnetic property before and after the conjugation. In addition, the composition of VMNPs was quantitively determined using the data provided from the ICP-AES, CE %, and LE %.

*3.1.1. Conjugation of VM to MNPs.* MNPs were chemically conjugated with VM via DSS through a multi-step process including the synthesis of APTMS−TEOS-coated MNPs.[29,31] Generally, solid-state NMR is recommended to evaluate conjugation efficiency. However, FTIR analysis was used for evaluation due to the lack of availability of solid-state NMR. The success of MNPs' functionalization process was assured using the FTIR spectrum of each constituent step (Figure 3).

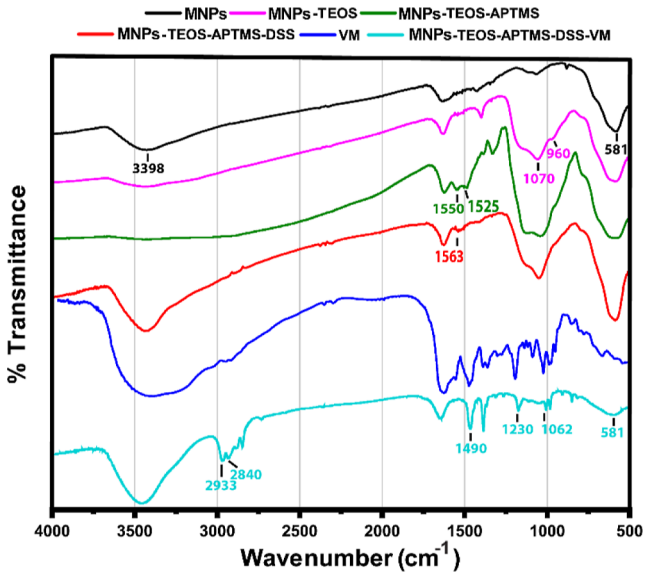


**Figure 3.** FTIR spectrum of VM, MNPs, TEOS, APTMS, and DSS, the multi-step synthesis procedure used on conjugating VM on MNPs.

At first, the synthesis of MNPs using the co-precipitation method was confirmed upon the presence of the characteristic Fe−O stretching peak at ∼581 $cm^{-1}$. The MNP spectrum also showed a peak at ∼3398 $cm^{-1}$, indicating the presence of OH surface layer on MNPs because of the high dielectric constant of deoxygenated water used in dissolving $FeCl_2$ and $FeCl_3$.[34] The formation of the $SiO_2$ layer on MNPs was confirmed by the presence of both the Si−O symmetric stretching peak at ∼1070 $cm^{-1}$ and the Si−O−Si stretching shoulder at ∼960 $cm^{-1}$.[35,36] The spectrum of MNPs−TEOS−APTMS showed characteristic peaks of $NH_2$ groups formed on the $SiO_2$ coating layer. These peaks include a peak at ∼1525 $cm^{-1}$ which is assigned to the N−H bending mode and a sharper peak at ∼1550 $cm^{-1}$ ascribed to the C−N vibration mode.[37] In addition, the peaks of Fe−O stretching, Si−O symmetric stretching, and Si−O−Si stretching are still observed in the MNPs−TEOS−APTMS FTIR spectrum, which demonstrates the successful conjugation of APTMS on the surface of $SiO_2$-coated MNPs.

The next step involves the utilization of the double cross-linker DSS on conjugating VM to the system. DSS reacts with $NH_2$ groups on both VM and MNPs−TEOS−APTMS, forming an amide bond on each side leaving the *N*-hydroxysuccinimide group. The FTIR spectrum of MNPs−TEOS−APTMS−DSS confirmed that conjugation by the presence of a sharp peak at ∼1563 $cm^{-1}$ which is attributed to the bending and scissoring of the NH group of the amide bond.[38] The final spectrum of VMNPs showed characteristic peaks of VM (1062, 1230, and 1490 $cm^{-1}$) that were not present in the preceding steps' spectra. In addition, the peak shape of VMNPs at ∼3400 $cm^{-1}$ looked more similar to the MNPs−TEOS−APTMS−DSS spectrum than the VM one and the peak intensity was in between its value in the aforementioned spectra supporting the successful conjugation of VM.[39−41] Those observations align with Jiang et al. (2021) who conjugated VM on PAMAM dendrimers and got evidence on the successful conjugation by the appearance of VM characteristic peaks on the conjugated VM−PAMAM dendrimer and the shape change in the overlapped 3400 $cm^{-1}$ peak.[42]

*3.1.2. Size and Electron Diffraction Analysis.* The physicochemical properties of VMNPs were evaluated using different characterization techniques. The morphology, size, and electron diffraction of MNPs and VMNPs were investigated using HR-TEM (JEM-2100, JEOL Ltd. Japan). TEM micrographs showed nearly spherical particles with an average diameter of 16.3 ± 2.6 nm as analyzed by ImageJ software (Figure 4a). It was also evident that MNPs exhibit a polycrystalline structure with an interplanar spacing of 0.4 nm as measured by the selected area electron diffraction (SAED) mode in HR-TEM (Figure 4b−d). Besides, the micrographs showed a clear coating by TEOS surrounding MNPs with a 5 nm thickness (Figure 4e). The silica layer is crucial as it stabilizes MNPs, prevents particle aggregation, and confers more functional groups for surface modification.[43] However, if the silica coating is too thick, it may potentially shield the magnetic character of MNPs. To accomplish this balance, we used a ratio of 1:2 TEOS to MNPs, respectively, based on an optimization reported by Thangaraj et al. (2019) where that ratio did not significantly affect the magnetization of MNPs as showed by VSM analysis.[30] A polycrystalline structure was also observed by the SAED mode in HR-TEM (Figure 4f). Upon completing the whole functionalization, the coating thickness increased to 8 nm which is possibly attributed to the addition of the other functionalization components (APTMS, DSS, and VM) (Figure 4g). It was also exhibiting a polycrystalline structure by SAED (Figure 4h).

*3.1.3. Magnetic Behavior.* Coated-MNPs were examined for their magnetic response by exposure to different external magnetic fields using VSM (Lake Shore model 7410, USA). The purpose of the examination is to investigate the impact of the coating on the inherent magnetic response of MNPs. The hysteresis loop and saturation magnetization of MNPs and MNPs−TEOS were compared, as shown in Figure 4i. MNPs showed a saturation magnetization value of 60 emu/g, whereas MNPs−TEOS presented a slightly lower value of around 51 emu/g (Figure 4j). This result indicates a 15% reduction in the magnetic character for coated-MNPs compared to free MNPs suggesting that MNPs' coating had only a mild effect on the magnetic property. The values of the saturation magnetization align with previous studies reporting the development of magnetic responsive systems to be used for therapeutic


https://doi.org/10.1021/acsomega.2c03226
ACS Omega 2022, 7, 30161−30170

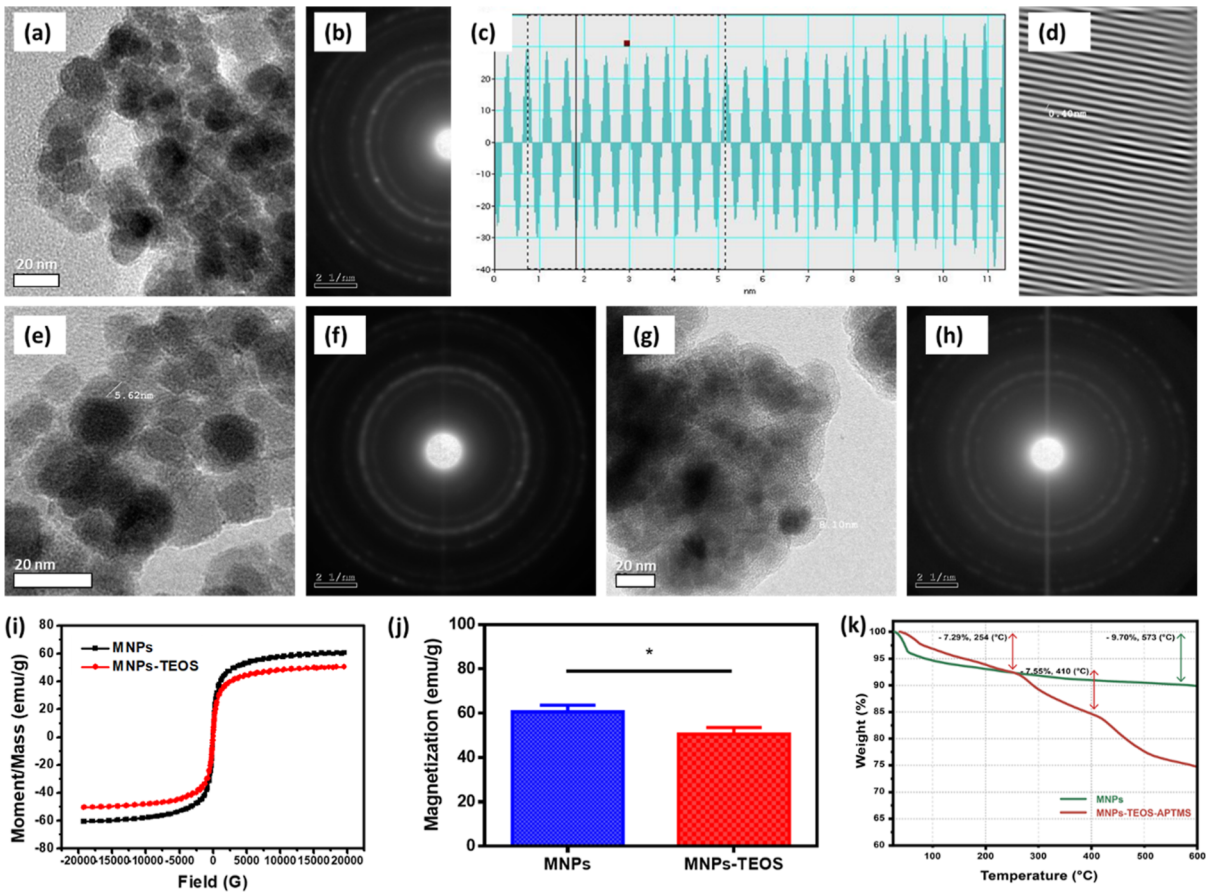


**Figure 4.** Functionalization of MNPs: TEM micrograph and SAED pattern of (a–d) MNPs, (e,f) TEOS-coated MNPs, and (g,h) VM-conjugated MNPs. Magnetic behavior (i) hysteresis loop, (j) saturation magnetization values (emu/g) of MNPs, and TEOS-coated MNPs. (k) TGA thermogram of MNPs and APTMS–TEOS-coated MNPs (MNPs–TEOS–APTMS). (*$p$ < 0.05, and $n$ = 3).

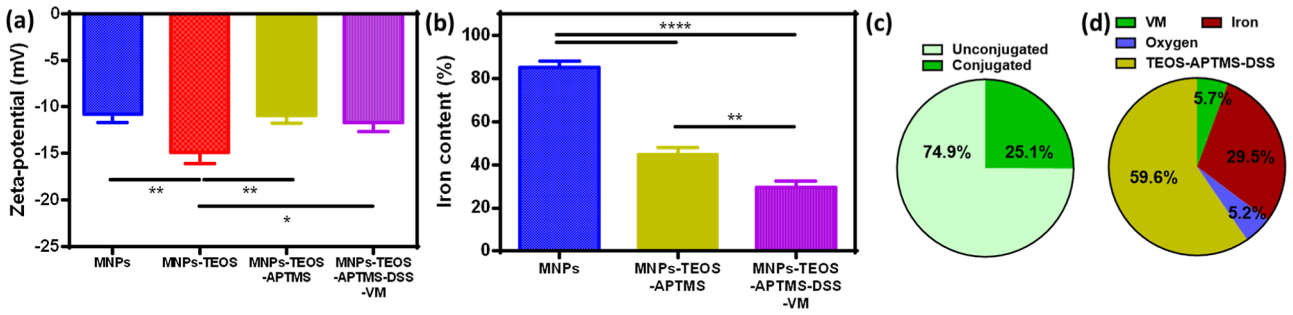


**Figure 5.** Characterization of VM-conjugated MNPs: (a) ζ-potential of different synthesis stages of VM-conjugated MNPs, VM, MNPs, DSS, TEOS, and APTMS. (b) Iron content percentage of MNPs, MNPs–TEOS–APTMS, VMNPs (MNPs–TEOS–APTMS–DSS–VM), (c) conjugation efficiency of VM, and (d) composition percentage of VM-conjugated MNPs (*$p$ < 0.05, **$p$ < 0.01, ****$p$ < 0.0001 and $n$ = 3).

hyperthermia. For example, Hayashi et al. reported the development of a hybrid MNP-organic system for magnetic responsive drug release. This system had a magnetic saturation value of 51 emu $g^{-1}$. The system was capable of producing a hyperthermia effect by increasing the temperature of the medium by 5.5 °C in 12 min.[44,45] Accordingly, this indicates the potential of the developed conjugate system to be used for targeted delivery or therapeutic hyperthermia using external magnetic field. It is also worth mentioning that MNPs with diameters below 30 nm were frequently reported to exhibit superparamagnetic properties.[46−48]

*3.1.4. Thermal Behavior.* TGA was utilized to examine the difference in the thermal behavior of MNPs and functionalized MNPs. Around 7 mg of each sample was exposed to a temperature range from room temperature (25 °C) until 600 °C, with a heating rate of 10 °C/min under nitrogen conditions. The weight loss percentage was measured for each corresponding temperature and plotted for comparison, as shown in Figure 4k. For MNPs, a single weight loss of 9.70% was observed around 573 °C which could be ascribed to the adsorbed water molecules and unreacted residues removal as well.[49,50] Functionalized MNPs exhibited two-weight losses. The first loss was 7.29% at 253.5 °C, which is ascribed to the breaking apart of aminopropyl groups on the surface of silica-coated MNPs.[48,51] While the second began at 409.7 °C and continued to 600 °C with a loss percentage of 7.55%, which is


https://doi.org/10.1021/acsomega.2c03226
ACS Omega 2022, 7, 30161−30170

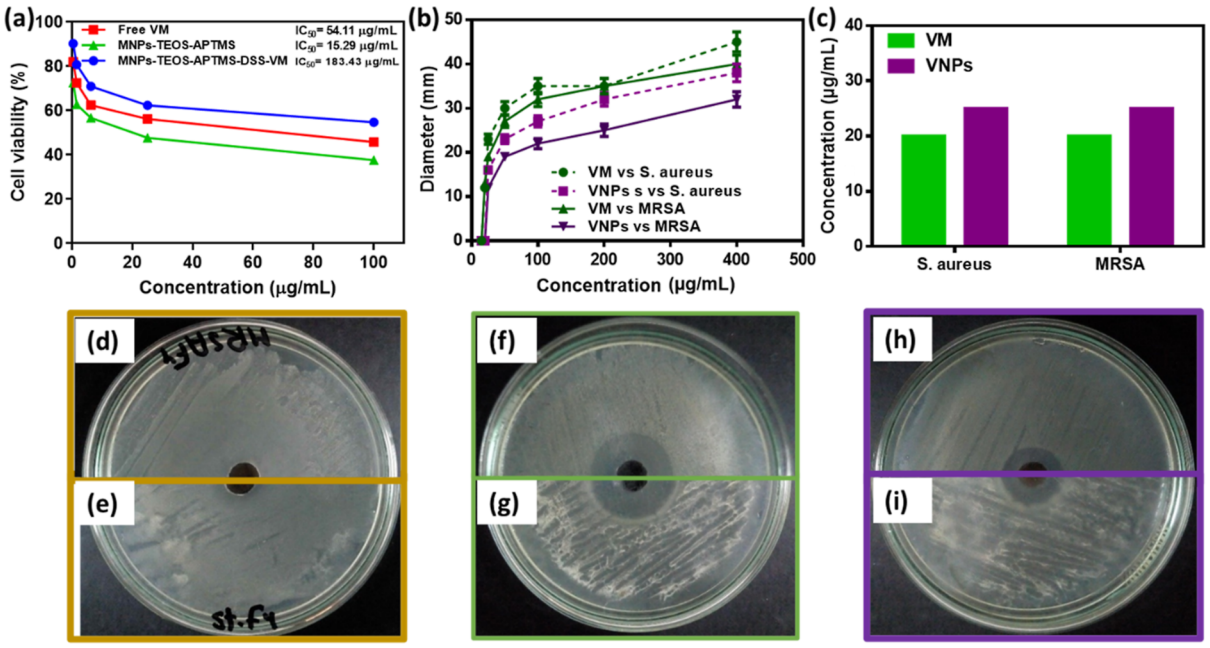


**Figure 6.** In vitro applications: (a) MTT cytotoxicity assay on WI-38 cells (fibroblasts human cell line from lung tissue) for VM, APTMS−TEOS-coated MNPs (MNPs−TEOS−APTMS), VM-conjugated MNPs (MNPs−TEOS−APTMS−DSS−VM). (b) Antibacterial activity using the agar diffusion method for VM and VMNPs against *S. aureus* and MRSA. (c) MIC for VM and VMNPs against *S. aureus* and MRSA. Image of the representative agar plate of MNPs−TEOS−APTMS against (d) MRSA and (e) *S. aureus*, VM at 25 $\mu$g/mL against (f) MRSA and (g) *S. aureus*, VMNPs at an equivalent VM concentration of 25 $\mu$g/mL against (h) MRSA and (i) *S. aureus*.

reported to accompany the decomposition of the silica layer.[52] These findings confirm the thermal stability of functionalized MNPs and support the successful coating of MNPs with a silica layer.

*3.1.5. Zeta Potential.* The charge of the different stages of VMNPs was measured using $\zeta$ potential (Nano-ZS, Malvern Instruments, Malvern, UK). As shown in Figure 5a, MNPs demonstrated a negative charge of −10.8 ± 0.85 mV which may be attributed to the residual ammonia used in producing $Fe_3O_4$ from the iron precursor. After the addition of the $SiO_2$ layer, the charge became more negative (−14.9 ± 1.17 mV) possibly due to the presence of hydroxyl groups resulting from the high dielectric constant of the used water.[34] Upon the conjugation of APTMS, the charge became less negative (−10.9 ± 0.85 mV) due to the presence of positive amine groups on the APTMS end. However, the charge was expected to be more positive than observed, this may be attributed to low APTMS concentration on the MNP surface. Shebl et al. (2017) tried a similar procedure to ours, but for conjugating APTMS directly onto MNPs in two reaction conditions, cold and hot. They found out that cold conditions were more efficient in coating MNPs as expressed in the change in the $\zeta$ potential of MNPs (from −18 to +24 for cold compared to −11 for hot conditions).[53] This might account for the small change in charge observed with the current study. Although VM is known to be positively charged at neutral pH,[54] the charge was observed to be almost the same as in MNPs−TEOS−APTMS. This result aligns with the previous interpretation of low APTMS concentration on the MNP surface. We plan to work on increasing the APTMS concentration, and so CE % of VM, in a future study.

*3.1.6. Iron Content Analysis.* The iron content was quantitatively determined in MNPs, MNPs−TEOS−APTMS, and VMNPs using ICP-AES [Agilent 5100 Synchronous Vertical Dual View (SVDV), CA, USA]. A sample of 2 mg/mL MNPs was analyzed using the ICP-AES, and the iron concentration was found to be 1.70 ± 0.03 mg/mL representing 85% of the whole MNPs (Figure 5b). For MNPs−TEOS−APTMS and VMNPs, the iron content was measured to account for 44.9 and 29.5%, respectively. This result follows the reported range of iron content for MNPs. For instance, Wu et al. (2011) reported that the iron content of MNPs to be around 70% using EDS analysis.[55] There is a clear reduction of the iron content as we go from MNPs to VMNPs which supports the successful conjugation.

*3.1.7. Percent Composition of VM-Conjugated MNPs.* The CE % of VM on MNPs was determined indirectly by measuring the absorbance of VM in the supernatant at 279.8 nm. Using the calibration curve, the amount of conjugated VM could be figured out by subtracting the unconjugated from the initial VM amount. CE % was found to be 25.1% (Figure 5c), while LE % was calculated to be 5.7% following triplicate measurements (Figure 5d). These low values may be attributed to a small concentration of APTMS on the MNP surface as discussed before. We plan to optimize the reaction conditions and CE % in a future study. The percent composition of VMNPs was determined based on the iron content data and VM LE %, as shown in Figure 5b−d. The predominant species of the particles was the connecting molecules, which is TEOS−APTMS−DSS with a percentage of 59.6%. Meanwhile, oxygen represents 5.2%, which is given from its percentage in the pure MNPs.

**3.2. Applications.** At first, the cytotoxicity profile of VMNPs was studied against the normal lung cell line, WI-38 human diploid lung fibroblast. The therapeutic efficiency was then evaluated by measuring the bactericidal activity against two frequent Gram-positive strains, *S. aureus* and MRSA.

*3.2.1. In Vitro Cell Biocompatibility Study.* The cytotoxicity profile of VMNPs was assessed in vitro against WI-38 human diploid lung fibroblast. Utilizing the MTT assay, the associated


https://doi.org/10.1021/acsomega.2c03226
ACS Omega 2022, 7, 30161−30170

NPs cytotoxicity was demonstrated from studying the change in the cell viability percentage while varying the compounds and their concentration. As shown in Figure 6a, the cell viability showed a moderate decrease as the concentration of VMNPs increased. The $IC_{50}$ of VMNPs was measured to be 183.43 $\mu$g/mL, compared to a lower value of 54.11 $\mu$g/mL associated with free VM. This difference in $IC_{50}$ values reflects that the conjugation of VM helps decrease the cytotoxicity of the drug. Such an effect was also observed by Gounani et al., where they loaded VM and polymyxin B to mesoporous silica nanoparticles. They showed that loading antibiotics to nano drug delivery carrier enhanced the biocompatibility of those drugs as demonstrated by the MTT assay.[56] On the other hand, MNPs−TEOS−APTMS was found to be more cytotoxic with $IC_{50}$ of 15.29 $\mu$g/mL, which may be attributed to the charged amine groups present on APTMS. To mitigate this toxicity, it is required to conjugate MNPs−TEOS−APTMS with opposite-charged molecules such as DSS−VM that are rich with negative carboxylate groups. Therefore, VMNPs were found to have much better biocompatibility on WI-38 human diploid lung fibroblast, which heralded a better safety profile.

*3.2.2. In Vitro Antibacterial Activity Evaluation.* The antibacterial activity of VMNPs was assessed by measuring the inhibition zone diameter of bacterial growth. The developed VMNPs were examined against two Gram-positive bacterial strains, *S. aureus* and MRSA. The antibacterial results were compared to free VM to evaluate the difference in activity, as shown in Figure 6b. The results showed that VM exhibits lower MIC for *S. aureus* and MRSA (20 $\mu$g/mL), compared to 25 $\mu$g/mL for VMNPs against both strains (Figure 6c). Moreover, functionalized MNPs without VM (MNPs−TEOS−APTMS) did not show significant activity against either bacterial strain (Figure 6d,e). This observation asserts that the key contributor in the measured bactericidal activity is VM. Photographic images for agar plates of free VM at 25 $\mu$g/mL concentration showed a inhibition zone with 22 mm diameter and 19 mm diameter against *S. aureus* and MRSA, respectively (Figure 6f,g). Meanwhile, the inhibition zone diameter of VMNPs at equivalent VM concentration of 25 $\mu$g/mL was measured to be 16 and 14 mm against *S. aureus* and MRSA, respectively (Figure 6h,i). VM's mode of action relies on inhibiting the cell wall synthesis of Gram-positive bacteria through the electrostatic interaction between the positive amine groups of VM and the negative groups of the D-Ala-D-Ala terminal in peptidoglycans.[57] This involvement of VM's amine groups in the antibacterial activity may interpret the observed difference in activity between free VM and VMNPs, where VMNPs exhibit less free amine groups given that some of them were consumed into the conjugation with MNPs. However, the difference in antibacterial activity was just moderate, suggesting a comparable antibacterial activity. On the other hand, the biocompatibility of VMNPs was much better than free VM. These findings impose the promising use of VMNPs as an alternative for free VM as it provides a comparable antibacterial activity and better biocompatibility.

## 4. CONCLUSIONS

In the reported study, VM was conjugated to the surface of MNPs using a multistep approach. The NPs were initially coated with a silica layer, followed by linker addition, and then finally conjugating the VM peptide. Conjugation of VM on the MNP core provides a dual level of targeting. The first targeting strategy is the D-Ala-D-Ala binding moiety, which allows irreversible binding of VM to bacterial cell walls. Meanwhile, the external magnetic field can be used to localize the conjugated system to the target organ and minimize the leakage into systemic circulation. The developed VMNPs showed comparable activity to free VM but with better biocompatibility, which may minimize the associated side effects of the systemic administration of VM. A future study will focus on proving the active targeting of the developed formulation.

## AUTHOR INFORMATION


### Corresponding Author

**Islam A. Khalil** − *Department of Pharmaceutics, College of Pharmaceutical Sciences and Drug Manufacturing, Misr University of Science and Technology (MUST), 6th of October, Giza 12582, Egypt;* orcid.org/0000-0002-6804-4144; Phone: +201090140748; Email: islam.khalil@must.edu.eg

### Authors

**Moustafa M. Abdelaziz** − *Department of Bioengineering, The University of Kansas, Lawrence, Kansas 66045, United States;* orcid.org/0000-0002-0098-5749

**Amr Hefnawy** − *Smyth Laboratory, College of Pharmacy, University of Texas at Austin, Austin, Texas 78712, United States*

**Asem Anter** − *Microbiology Unit, Drug Factory, College of Pharmaceutical Sciences and Drug Manufacturing, Misr University of Science and Technology (MUST), 6th of October, Giza 12582, Egypt*

**Menna M. Abdellatif** − *Department of Industrial Pharmacy, College of Pharmaceutical Sciences and Drug Manufacturing, Misr University for Science and Technology, Giza 12582, Egypt*

**Mahmoud A. F. Khalil** − *Department of Microbiology and Immunology, Faculty of Pharmacy, Fayoum University, Fayoum 63514, Egypt*

Complete contact information is available at: https://pubs.acs.org/10.1021/acsomega.2c03226


### Author Contributions

M.M.A. and A.H.: methodology, data curation, formal analysis, investigation, writing—original draft, writing—review and editing, and visualization. A.A.: methodology, data curation, formal analysis, investigation, and writing—original draft. M.M.A. and M.A.F.K.: conceptualization, methodology. I.A.K.: conceptualization, methodology, data curation, formal analysis, investigation, writing—original draft, writing—review and editing, visualization, funding acquisition, and project administration.


### Funding

I.A.K. acknowledges the Science, Technology & Innovation Funding Authority (STIFA/STDF) under grants 30084 (PI Khalil) for full support of this work.


### Notes

The authors declare no competing financial interest.

## REFERENCES


(1) Baptista, P. V.; McCusker, M. P.; Carvalho, A.; Ferreira, D. A.; Mohan, N. M.; Martins, M.; Fernandes, A. R. Nano-Strategies to Fight Multidrug Resistant Bacteria-"A Battle of the Titans". *Front. Microbiol.* **2018**, *9*, 1−26.

(2) Ding, X.; Wang, A.; Tong, W.; Xu, F. J. Biodegradable Antibacterial Polymeric Nanosystems: A New Hope to Cope with Multidrug-Resistant Bacteria. *Small* **2019**, *15*, 1900999.
(3) Rai, M. K.; Deshmukh, S. D.; Ingle, A. P.; Gade, A. K. Silver Nanoparticles: The Powerful Nanoweapon against Multidrug-Resistant Bacteria. *J. Appl. Microbiol.* **2012**, *112*, 841−852.
(4) Chen, C. W.; Hsu, C. Y.; Lai, S. M.; Syu, W. J.; Wang, T. Y.; Lai, P. S. Metal Nanobullets for Multidrug Resistant Bacteria and Biofilms. *Adv. Drug Delivery Rev.* **2014**, *78*, 88−104.
(5) Kalishwaralal, K.; BarathManiKanth, S.; Pandian, S. R. K.; Deepak, V.; Gurunathan, S. Silver Nanoparticles Impede the Biofilm Formation by Pseudomonas Aeruginosa and Staphylococcus Epidermidis. *Colloids Surf., B* **2010**, *79*, 340−344.
(6) Li, Z.; Bai, H.; Jia, S.; Yuan, H.; Gao, L. H.; Liang, H. Design of Functional Polymer Nanomaterials for Antimicrobial Therapy and Combatting Resistance. *Mater. Chem. Front.* **2021**, *5*, 1236−1252.
(7) Wang, X.; Cui, Q.; Yao, C.; Li, S.; Zhang, P.; Sun, H.; Lv, F.; Liu, L.; Li, L.; Wang, S. Conjugated Polyelectrolyte−Silver Nanostructure Pair for Detection and Killing of Bacteria. *Adv. Mater. Technol.* **2017**, *2*, 1700033.
(8) Li, W.; Separovic, F.; O'Brien-Simpson, N. M.; Wade, J. D. Chemically Modified and Conjugated Antimicrobial Peptides against Superbugs. *Chem. Soc. Rev.* **2021**, *50*, 4932−4973.
(9) Lombardi, L.; Falanga, A.; Del Genio, V.; Galdiero, S. A New Hope: Self-Assembling Peptides with Antimicrobial Activity. *Pharmaceutics* **2019**, *11*, 166.
(10) Butler, M. S.; Hansford, K. A.; Blaskovich, M. A. T.; Halai, R.; Cooper, M. A. Glycopeptide Antibiotics: Back to the Future. *J. Antibiot.* **2014**, *67*, 631−644.
(11) Pasupuleti, M.; Schmidtchen, A.; Malmsten, M. Antimicrobial Peptides: Key Components of the Innate Immune System. *Crit. Rev. Biotechnol.* **2012**, *32*, 143−171.
(12) Vazquez-Guillamet, C.; Kollef, M. H. Treatment of Gram-Positive Infections in Critically Ill Patients. *BMC Infect. Dis.* **2014**, *14*, 92.
(13) Shime, N.; Kato, Y.; Kosaka, T.; Kokufu, T.; Yamagishi, M.; Fujita, N. Glycopeptide Pharmacokinetics in Current Paediatric Cardiac Surgery Practice. *Eur. J. Cardio-Thorac. Surg.* **2007**, *32*, 577−581.
(14) Omardien, S.; Brul, S.; Zaat, S. A. J. Antimicrobial Activity of Cationic Antimicrobial Peptides against Gram-Positives: Current Progress Made in Understanding the Mode of Action and the Response of Bacteria. *Front. Cell Dev. Biol.* **2016**, *4*, 1−16.
(15) Sundram, U. N.; Griffin, J. H.; Nicas, T. I. Novel Vancomycin Dimers with Activity against Vancomycin-Resistant Enterococci. *J. Am. Chem. Soc.* **1996**, *118*, 13107−13108.
(16) Aoki, Y.; Kashiwagi, H. Bactericidal Activity of Vancomycin against Methicillin-Resistant Staphylococcus Aureus (MRSA): Comparison with Minocycline and Ofloxacin within Therapeutic Levels, and Factors Determining Their Efficacy. *Chemotherapy* **1992**, *40*, 997−1004.
(17) Gu, H.; Ho, P.-L.; Tsang, K. W. T.; Wang, L.; Xu, B. Using Biofunctional Magnetic Nanoparticles to Capture Vancomycin-Resistant Enterococci and Other Gram-Positive Bacteria at Ultralow Concentration. *J. Am. Chem. Soc.* **2003**, *125*, 15702−15703.
(18) Kinik, H.; Karaduman, M. Cierny-Mader Type III Chronic Osteomyelitis: The Results of Patients Treated with Debridement, Irrigation, Vancomycin Beads and Systemic Antibiotics. *Int. Orthop.* **2008**, *32*, 551−558.
(19) Bakhsheshi-Rad, H. R.; Hamzah, E.; Ismail, A. F.; Aziz, M.; Hadisi, Z.; Kashefian, M.; Najafinezhad, A. Novel Nanostructured Baghdadite-Vancomycin Scaffolds: In-Vitro Drug Release, Antibacterial Activity and Biocompatibility. *Mater. Lett.* **2017**, *209*, 369−372.
(20) Healy, D. P.; Sahai, J. V.; Fuller, S. H.; Polk, R. E. Vancomycin-Induced Histamine Release and "Red Man Syndrome": Comparison of 1- and 2-Hour Infusions. *Antimicrob. Agents Chemother.* **1990**, *34*, 550−554.
(21) Mou, X.; Ali, Z.; Li, S.; He, N. Applications of Magnetic Nanoparticles in Targeted Drug Delivery System. *J. Nanosci. Nanotechnol.* **2015**, *15*, 54−62.
(22) Sadhukha, T.; Wiedmann, T. S.; Panyam, J. Inhalable Magnetic Nanoparticles for Targeted Hyperthermia in Lung Cancer Therapy. *Biomaterials* **2013**, *34*, 5163−5171.
(23) Ho, D.; Sun, X.; Sun, S. Monodisperse Magnetic Nanoparticles for Theranostic Applications. *Acc. Chem. Res.* **2011**, *44*, 875−882.
(24) Li, S.; Mason, C. E.; Melnick, A. Genetic and Epigenetic Heterogeneity in Acute Myeloid Leukemia. *Curr. Opin. Genet. Dev.* **2016**, *36*, 100−106.
(25) Zaloga, J.; Janko, C.; Nowak, J.; Matuszak, J.; Knaup, S.; Eberbeck, D.; Tietze, R.; Unterweger, H.; Friedrich, R. P.; Heimke-Brinck, S.; Baum, R.; Cicha, E.; Dorje, I.; Odenbach, F.; Lyer, S.; Lee, S.; Alexiou, G.; Duerr, C. Development of a Lauric Acid/Albumin Hybrid Iron Oxide Nanoparticle System with Improved Biocompatibility. *Int. J. Nanomed.* **2014**, *9*, 4847−4866.
(26) Zhang, W.; Taheri-Ledari, R.; Hajizadeh, Z.; Zolfaghari, E.; Ahghari, M. R.; Maleki, A.; Hamblin, M. R.; Tian, Y. Enhanced Activity of Vancomycin by Encapsulation in Hybrid Magnetic Nanoparticles Conjugated to a Cell-Penetrating Peptide. *Nanoscale* **2020**, *12*, 3855−3870.
(27) Rashid, M.; Rabbi, M. A.; Ara, T.; Hossain, M. M.; Islam, M. S.; Elaissari, A.; Ahmad, H.; Rahman, M. M. Vancomycin Conjugated Iron Oxide Nanoparticles for Magnetic Targeting and Efficient Capture of Gram-Positive and Gram-Negative Bacteria. *RSC Adv.* **2021**, *11*, 36319−36328.
(28) Jabalera, Y.; Montalban-Lopez, M.; Vinuesa-Rodriguez, J. J.; Iglesias, G. R.; Maqueda, M.; Jimenez-Lopez, C. Antibacterial Directed Chemotherapy Using AS-48 Peptide Immobilized on Biomimetic Magnetic Nanoparticles Combined with Magnetic Hyperthermia. *Int. J. Biol. Macromol.* **2021**, *189*, 206−213.
(29) Lin, Y. S.; Tsai, P. J.; Weng, M. F.; Chen, Y. C. Affinity Capture Using Vancomycin-Bound Magnetic Nanoparticles for the MALDI-MS Analysis of Bacteria. *Anal. Chem.* **2005**, *77*, 1753−1760.
(30) Thangaraj, B.; Jia, Z.; Dai, L.; Liu, D.; Du, W. Effect of Silica Coating on Fe3O4 Magnetic Nanoparticles for Lipase Immobilization and Their Application for Biodiesel Production. *Arabian J. Chem.* **2019**, *12*, 4694−4706.
(31) Wan, Y.; Zhang, D.; Hou, B. Determination of Sulphate-Reducing Bacteria Based on Vancomycin-Functionalised Magnetic Nanoparticles Using a Modification-Free Quartz Crystal Microbalance. *Biosens. Bioelectron.* **2010**, *25*, 1847−1850.
(32) Jahangirian, H.; Haron, M. J.; Shah Ismail, M. H.; Rafiee-Moghaddam, R.; Afsah-Hejri, L.; Abdollahi, Y.; Rezayi, M.; Vafaei, N. Well Diffusion Method for Evaluation of Antibacterial Activity of Copper Phenyl Fatty Hydroxamate Synthesized from Canola and Palm Kernel Oils. *Dig. J. Nanomater. Biostructures* **2013**, *8*, 1263−1270.
(33) Akanbi, O. E.; Njom, H. A.; Fri, J.; Otigbu, A. C.; Clarke, A. M. Antimicrobial Susceptibility of Staphylococcus Aureus Isolated from Recreational Waters and Beach Sand in Eastern Cape Province of South Africa. *Int. J. Environ. Res. Public Health* **2017**, *14*, 1001.
(34) Jalilian, A. R.; Panahifar, A.; Mahmoudi, M.; Akhlaghi, M.; Simchi, A. Preparation and Biological Evaluation of [67Ga]-Labeled-Superparamagnetic Nanoparticles in Normal Rats. *Radiochim. Acta* **2009**, *97*, 51−56.
(35) Shafqat, S. S.; Khan, A. A.; Zafar, M. N.; Alhaji, M. H.; Sanaullah, K.; Shafqat, S. R.; Murtaza, S.; Pang, S. C. Development of Amino-Functionalized Silica Nanoparticles for Efficient and Rapid Removal of COD from Pre-Treated Palm Oil Effluent. *J. Mater. Res. Technol.* **2019**, *8*, 385−395.
(36) Jiang, Y.; Shi, L.; Huang, Y.; Gao, J.; Zhang, X.; Zhou, L. Preparation of Robust Biocatalyst Based on Cross-Linked Enzyme Aggregates Entrapped in Three-Dimensionally Ordered Macroporous Silica. *ACS Appl. Mater. Interfaces* **2014**, *6*, 2622−2628.
(37) Yang, L.; Tian, J.; Meng, J.; Zhao, R.; Li, C.; Ma, J.; Jin, T. Modification and Characterization of Fe3O4 Nanoparticles for Use in Adsorption of Alkaloids. *Molecules* **2018**, *23*, 562.


https://doi.org/10.1021/acsomega.2c03226
*ACS Omega* 2022, 7, 30161−30170

(38) Zhao, X.; Wang, J.; Song, Y.; Chen, X. Synthesis of Nanomedicines by Nanohybrids Conjugating Ginsenosides with Auto-Targeting and Enhanced MRI Contrast for Liver Cancer Therapy. *Drug Dev. Ind. Pharm.* **2018**, *44*, 1307−1316.
(39) Lankalapalli, S.; Tenneti, V. S. V. K.; Nimmali, S. K. Design and Development of Vancomycin Liposomes. *Indian J. Pharm. Educ. Res.* **2015**, *49*, 208−215.
(40) Cerchiara, T.; Abruzzo, A.; di Cagno, M.; Bigucci, F.; Bauer-Brandl, A.; Parolin, C.; Vitali, B.; Gallucci, M. C.; Luppi, B. Chitosan Based Micro- and Nanoparticles for Colon-Targeted Delivery of Vancomycin Prepared by Alternative Processing Methods. *Eur. J. Pharm. Biopharm.* **2015**, *92*, 112−119.
(41) Giammarco, J.; Mochalin, V. N.; Haeckel, J.; Gogotsi, Y. The Adsorption of Tetracycline and Vancomycin onto Nanodiamond with Controlled Release. *J. Colloid Interface Sci.* **2016**, *468*, 253−261.
(42) Jiang, G.; Liu, S.; Yu, T.; Wu, R.; Ren, Y.; van der Mei, H. C.; Liu, J.; Busscher, H. J. PAMAM Dendrimers with Dual-Conjugated Vancomycin and Ag-Nanoparticles Do Not Induce Bacterial Resistance and Kill Vancomycin-Resistant Staphylococci. *Acta Biomater.* **2021**, *123*, 230−243.
(43) Kunzmann, A.; Andersson, B.; Vogt, C.; Feliu, N.; Ye, F.; Gabrielsson, S.; Toprak, M. S.; Buerki-Thurnherr, T.; Laurent, S.; Vahter, M.; Krug, H.; Muhammed, M.; Scheynius, A.; Fadeel, B. Efficient Internalization of Silica-Coated Iron Oxide Nanoparticles of Different Sizes by Primary Human Macrophages and Dendritic Cells. *Toxicol. Appl. Pharmacol.* **2011**, *253*, 81−93.
(44) Hayashi, K.; Ono, K.; Suzuki, H.; Sawada, M.; Moriya, M.; Sakamoto, W.; Yogo, T. High-Frequency, Magnetic-Field-Responsive Drug Release from Magnetic Nanoparticle/Organic Hybrid Based on Hyperthermic Effect. *ACS Appl. Mater. Interfaces* **2010**, *2*, 1903−1911.
(45) Kandasamy, G.; Sudame, A.; Bhati, P.; Chakrabarty, A.; Maity, D. Systematic Investigations on Heating Effects of Carboxyl-Amine Functionalized Superparamagnetic Iron Oxide Nanoparticles (SPIONs) Based Ferrofluids for in Vitro Cancer Hyperthermia Therapy. *J. Mol. Liq.* **2018**, *256*, 224−237.
(46) Zhi, J.; Wang, Y.; Lu, Y.; Ma, J.; Luo, G. In Situ Preparation of Magnetic Chitosan/Fe3O4 Composite Nanoparticles in Tiny Pools of Water-in-Oil Microemulsion. *React. Funct. Polym.* **2006**, *66*, 1552−1558.
(47) Khan, M. A.; Mujahid, M.; Chen, Z.; Kiani, F. A.; Chye, S.; Loo, J.; Guang, Y.; Lim, J. An Experimental and Theoretical Approach to Investigate Correlation between Electromagnetic Properties of Doped Ferrites & Its Interfacial Reactivity with Dopamine. *Appl. Surf. Sci.* **2020**, *506*, 144945.
(48) Wang, J.; Zheng, S.; Shao, Y.; Liu, J.; Xu, Z.; Zhu, D. Amino-Functionalized Fe3O4@SiO2 Core-Shell Magnetic Nanomaterial as a Novel Adsorbent for Aqueous Heavy Metals Removal. *J. Colloid Interface Sci.* **2010**, *349*, 293−299.
(49) Li, G.-y.; Huang, K. l.; Jiang, Y. r.; Ding, P.; Yang, D. l. Preparation and Characterization of Carboxyl Functionalization of Chitosan Derivative Magnetic Nanoparticles. *Biochem. Eng. J.* **2008**, *40*, 408−414.
(50) Li, L.; Mak, K. Y.; Leung, C. W.; Chan, K. Y.; Chan, W. K.; Zhong, W.; Pong, P. W. T. Synthesis and Characterization of Self-Assembled Monolayer and Bilayer Carboxyl-Group Functionalized Magnetic Nanoparticles. *IEEE Trans. Magn.* **2012**, *48*, 3299−3302.
(51) Lei, Z.; Li, Y.; Wei, X. A Facile Two-Step Modifying Process for Preparation of Poly(SStNa)-Grafted Fe3O4/SiO2 Particles. *J. Solid State Chem.* **2008**, *181*, 480−486.
(52) Naeimi, H.; Mohamadabadi, S. Sulfonic Acid-Functionalized Silica-Coated Magnetic Nanoparticles as an Efficient Reusable Catalyst for the Synthesis of 1-Substituted 1H-Tetrazoles under Solvent-Free Conditions. *Dalton Trans.* **2014**, *43*, 12967−12973.
(53) Shebl, R. I.; Farouk, F.; Azzazy, H. M. E. S. Effect of Surface Charge and Hydrophobicity Modulation on the Antibacterial and Antibiofilm Potential of Magnetic Iron Nanoparticles. *J. Nanomater.* **2017**, *2017*, 3528295.
(54) Takács-Novák, K.; Noszál, B.; Tókés-Kövesdi, M.; Szász, G. Acid-Base Properties and Proton-Speciation of Vancomycin. *Int. J. Pharm.* **1993**, *89*, 261−263.
(55) Wu, S.; Sun, A.; Zhai, F.; Wang, J.; Xu, W.; Zhang, Q.; Volinsky, A. A. Fe3O4 Magnetic Nanoparticles Synthesis from Tailings by Ultrasonic Chemical Co-Precipitation. *Mater. Lett.* **2011**, *65*, 1882−1884.
(56) Gounani, Z.; Asadollahi, M. A.; Pedersen, J. N.; Lyngsø, J.; Skov Pedersen, J.; Arpanaei, A.; Meyer, R. L. Mesoporous Silica Nanoparticles Carrying Multiple Antibiotics Provide Enhanced Synergistic e Ff Ect and Improved Biocompatibility. *Colloids Surf., B* **2019**, *175*, 498−508.
(57) Esmaeili, A.; Ghobadianpour, S. Vancomycin Loaded Super-paramagnetic MnFe 2 O 4 Nanoparticles Coated with PEGylated Chitosan to Enhance Antibacterial Activity. *Int. J. Pharm.* **2016**, *501*, 326−330.




https://doi.org/10.1021/acsomega.2c03226
*ACS Omega* 2022, 7, 30161−30170